Biosensors and Bioelectronics 250 (2024) 116040

Contents lists available at ScienceDirect

Biosensors and Bioelectronics

journal homepage: www.elsevier.com/locate/bios

High enhancement of sensitivity and reproducibility in label-free SARS-CoV-2 detection with graphene field-effect transistor sensors through precise surface biofunctionalization control

Laura Lozano-Chamizo [a,b,c], Carlos Márquez [d,e], Marzia Marciello [a,b], José Carlos Galdon [d,e], Elsa de la Fuente-Zapico [d,e], Paula Martinez-Mazón [d,e], Víctor Gonzalez-Rumayor [c], Marco Filice [a,b,*], Francisco Gamiz [d,e,**]

[a] Nanobiotechnology for Life Sciences Laboratory, Department of Chemistry in Pharmaceutical Sciences, Faculty of Pharmacy, Universidad Complutense de Madrid (UCM), Plaza Ramón y Cajal s/n, E-28040, Madrid, Spain
[b] Microscopy and Dynamic Imaging Unit, Fundación Centro Nacional de Investigaciones Cardiovasculares Carlos III (CNIC), Calle Melchor Fernández Almagro 3, E-28029, Madrid, Spain
[c] Atrys Health, E-28001, Madrid, Spain
[d] Nanoelectronics Research Group, Department of Electronics, CITIC-UGR (Research Center for Information and Communication Technologies), University of Granada, Spain
[e] Instituto de Investigación Biosanitaria de Granada ibs.GRANADA, 18012, Granada, Spain

ARTICLE INFO

Keywords:
Graphene field effect transistor
Biosensor
Oriented immobilization
2D materials
Nanobiotechnology
Antibody

ABSTRACT

The COVID-19 pandemic has taught us valuable lessons, especially the urgent need for a widespread, rapid and sensitive diagnostic tool. To this, the integration of bidimensional nanomaterials, particularly graphene, into point-of-care biomedical devices is a groundbreaking strategy able to potentially revolutionize the diagnostic landscape. Despite advancements in the fabrication of these biosensors, the relationship between their surface biofunctionalization and sensing performance remains unclear. Here, we demonstrate that the combination of careful sensor fabrication and its precise surface biofunctionalization is crucial for exalting the sensing performances of 2D biosensors. Specifically, we have biofunctionalized Graphene Field-Effect Transistor (GFET) sensors surface through different biochemical reactions to promote either random/heterogeneous or oriented/homogeneous immobilization of the Anti-SARS-CoV-2 spike protein antibody. Each strategy was thoroughly characterized by *in-silico* simulations, physicochemical and biochemical techniques and electrical characterization. Subsequently, both biosensors were tested in the label-free direct titration of SARS-CoV-2 virus in simulated clinical samples, avoiding sample preprocessing and within short timeframes. Remarkably, the oriented GFET biosensor exhibited significantly enhanced reproducibility and responsiveness, surpassing the detection sensitivity of conventional non-oriented GFET by more than twofold. This breakthrough not only involves direct implications for COVID-19 surveillance and next pandemic preparedness but also clarify an unexplored mechanistic dimension of biosensor research utilizing 2D-nanomaterials.

1. Introduction

On January 30, 2020, the World Health Organization (WHO) declared the COVID-19 pandemic, caused by severe acute respiratory syndrome coronavirus 2 (SARS-CoV-2), a Public Health Emergency of International Concern (Lu et al., 2020; Maia et al., 2022). Over the course of more than 3 years, there have been over 765 million confirmed cases and 6.9 million reported deaths worldwide (WHO, 2023). Although the WHO declared the end of the global health emergency on May 6, 2023, COVID-19 remains endemic. This new post-pandemic

* Corresponding author. Nanobiotechnology for Life Sciences Laboratory, Department of Chemistry in Pharmaceutical Sciences, Faculty of Pharmacy, Universidad Complutense de Madrid (UCM), Plaza Ramón y Cajal s/n, E-28040, Madrid, Spain.
** Corresponding author. Nanoelectronics Research Group, Department of Electronics, CITIC-UGR (Research Center for Information and Communication technologies), University of Granada, Spain.
E-mail addresses: mfilice@ucm.es (M. Filice), fgamiz@ugr.es (F. Gamiz).

https://doi.org/10.1016/j.bios.2024.116040
Received 28 September 2023; Received in revised form 14 December 2023; Accepted 12 January 2024
Available online 20 January 2024

phase requires the implementation of a comprehensive surveillance and monitoring strategy. The SARS-CoV-2 virus and its constantly emerging variants, which could trigger new surges, continue to pose a serious risk to our lives, especially for the at-risk population (Centers for Disease Control and Prevention, 2023). This approach is essential not only for the transition to the post-pandemic surveillance phase but especially for enhancing preparedness for future pandemics (G7 pandemic preparedness partnership, 2021).

One of the critical challenges highlighted during the early stages of the COVID-19 pandemic was the need for early, precise, and large-scale identification of infected individuals, especially frontline health workers and high-risk populations. Timely detection allows for appropriate treatment, preventive measures, and therapy administration to halt the spread of the disease.

The gold standard for detecting SARS-CoV-2 in COVID-19 is the quantitative reverse transcription-polymerase chain reaction (qRT-PCR) molecular test (Benzigar et al., 2021). However, despite its high accuracy, this method requires time-consuming sample preparation, specialized professionals and expensive equipment and reagents, which hinder its large-scale deployment for the rapid detection of potentially millions of infected individuals, turning the early large-scale diagnostic step into a critical bottleneck.

Rapid antigen detection tests (RADTs) offer an alternative as they provide quick results at the point of care (PoC) (Biagetti et al., 2023). However, RADTs have shown lower sensitivity, particularly in the early stages of the disease, leading to increased false negatives (Kohmer et al., 2021). Therefore, there is a need for novel highly sensitive methods combining the advantages of molecular tests (specificity and sensitivity) with those of RADTs (rapidity, easiness, low-cost and large availability).

Field-effect transistors (FET) biosensors, particularly those based on two-dimensional (2D) nanomaterials such as graphene, offer a promising solution (Chen et al., 2010; Filice et al., 2021; Jiang et al., 2020; Li et al., 2019). These biosensors enable easy, reliable, sensitive, and instantaneous measurements, making them suitable for clinical diagnosis, PoC testing, and on-site detection (Kang et al., 2021; Seo et al., 2020; Xu et al., 2022). Graphene Field Effect Transistors (GFETs) have gained prominence in this field due to their unique properties and excellent biocompatibility (Zhu et al., 2015). Nevertheless, despite the initial enthusiasm sparked by the proliferation of FET sensor publications on COVID detection (Alnaji et al., 2023; Seo et al., 2020), the lack of FDA approval for COVID FET sensors is a reality. This delay is mainly related to various challenges and considerations surrounding the approval process for new medical devices that compels the FDA to adapt its evaluation criteria as soon as new research results are published. In other terms, the novelty of the GFET technology requires a learning curve for regulators to understand its intricacies and potential risks. In fact, GFET biosensors comprises a new technology that still needs a deeply research and still present some challenges that hamper a possible approval by the FDA, such as the lack of a bandgap or problems in the reproducibility and scalability of fabrication and measurements. Additionally, achieving optimal biosensing performance requires precise surface biofunctionalization, an issue that has not been systematically explored yet.

With regards to the latter, because of the physical phenomena involved in the GFET operation (Lemme et al., 2007; Novoselov et al., 2004; Schwierz, 2010; Zhu et al., 2015), it is critical to develop a standardized surface functionalization strategy capable of promoting homogeneous and reproducible modification of sensor surface. This strategy is essential for achieving the best biosensing results, especially in terms of sensitivity, selectivity, and reproducibility.

Antibodies (Abs) are widely used bioreceptors for the development of GFET biosensors (Filice et al., 2021) because of their high specificity and widespread availability. To maximize recognition ability, particularly in terms of sensitivity and selectivity (Gao et al., 2022), the optimal Abs immobilization must promote their covalent bonding in a correctly standing oriented and homogeneously distributed manner (Lou et al., 2019; Ruiz et al., 2019). This approach will ensure the best biosensing ability and long-term stability of the sensor without affecting its electrical properties. In fact, under these controlled conditions, it is expected that a more homogeneous electric conductivity will be achieved, resulting in more sensitive measurements across the entire surface of the GFET biosensor. However, a literature survey related to GFET biosensing development reveals that these critical parameters have not been systematically analyzed (Rexha et al., 2023). Most published research works have primarily focused on optimizing the inherent physical properties of graphene. Mainly because of their high coupling efficiency and easiness, the most used techniques for biofunctionalization of GFET biosensors include physical adsorption or carbodiimide-mediated covalent coupling (Tam et al., 2017). However, both strategies show serious drawbacks, especially that they are not site specific and are characterized by promoting an uncontrolled random distribution of antibodies on the GFET surface (Romagnoli et al., 2023). As a result, the sensor is expected to be modified by a heterogeneous layer of Abs with random orientations (standing, sideway, lying or a mix of all), showing one or both fragment antigen-binding sites (Fab domains) distributed in a sterically hindered way and, therefore, finally leading to a reduced response in antibody biorecognition ability and graphene's sensing capability (Fig. S1) (Gao et al., 2022).

Consequently, the lack of control in biofunctionalization of GFET biosensors is expected to negatively impact on their intrinsic physical properties (*e.g.*, charge transport) and, ultimately, their sensing ability, particularly in terms of sensitivity and reproducibility.

To address this unresolved issue, this work focuses on studying the influence of surface biofunctionalization control on the diagnostic ability of graphene FET biosensors for the precise detection of SARS-CoV-2 virus. The study investigates the impact of site-selective *versus* random immobilization of an Immunoglobulin (IgG) anti-Spike protein antibody over the sensing surface of the GFET sensors (Fig. 1). Theoretical simulations are performed to analyze the influence on the GFET conductivity of the charge distribution generated on the sensor surface by different Abs immobilization strategies. Experimental studies will then be carried out to compare the selected orienting immobilization strategies (by using different pyrene derivatives) and their associated chemical reactions to promote each of them, while applying the same initial chemical modification (pyrene-mediated π-π stacking) to the pristine graphene layer. The analytical performances of site-selectively and randomly biofunctionalized GFET biosensors in the direct detection of the SARS-CoV-2 virus in clinical simulating samples will be evaluated and compared. Finally, a comprehensive physical and chemical characterization (using XPS, AFM, SEM, and Raman techniques) of both GFET surfaces will be performed to demonstrate the different orientation and distribution of Abs, establishing a direct correlation between Abs immobilization and the final biosensing performance.

2. Materials and methods

2.1. Materials

Dimethyl sulfoxide (DMSO) was from VWR International (Radnor, PA, USA). 1-Pyrenebutyric acid N-hydroxisuccinimide ester (PASE) was purchased in Santa Cruz Biotechnology (Dallas, TX, USA). 1-Pyrenebutyric hydrazide (PBH), sodium phosphate monobasic monohydrate for phosphate buffer and sodium periodate were from Merck (Darmstadt, Germany). Anti-SARS-CoV-2 spike glycoprotein antibody (ab272504) was purchased from Abcam (Cambridge, UK). Virus Transport Medium (VTM) was purchased form Condalab (Madrid, Spain). SARS-CoV-2 heat-inactivated (VR-1986HK) was purchased from ATCC (Manassas, VA, USA). The antibody concentrations were titrated by means of Coomassie Plus (Bradford) Assay Kit from ThemoFisher Scientific (Waltham, MA, USA) and following the instructions of the provider. Cooper foils were from Graphene Platform (Japan), 0.0035 mm thick and 99.95% purity. Gases were from Linde Gas H_2 5.0 and CH_4 5.0 purity. Poly

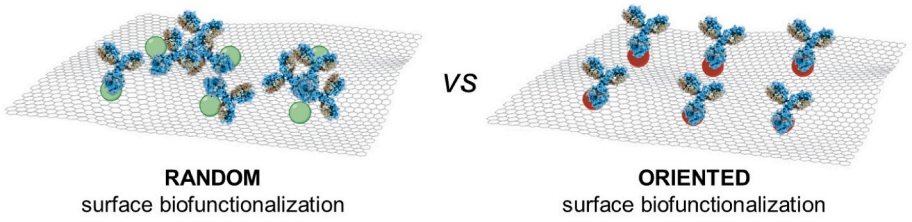

Fig. 1. General representation of GFET surface after random (rBioGFET) and oriented (oBioGFET) biofunctionalization.

(methyl methacrylate) (PMMA) was from Sigma Aldrich.

2.2. Simulation

The simulation of electronic devices provides insight into the physics of the device at a microscopic scale and helps to understand the observed experimental behaviour. In order to comprehend the experimental operation and explain the device's physical behaviour with the goal of improving its performance, we have simulated biosensor field-effect transistors (BioGFET) by adapting a commercial TCAD (Technology Computer Aided Design) simulation platform, specifically Sentaurus TCAD by Synopsys. The simulated device consists of graphene layer on top of a SiO_2/Si substrate. Ohmic metallic contacts have been considered to form drain and source contacts on top of the graphene layer. A Si_3N_4 passivation layer has been employed to contain the electrolyte and passivate the ohmic source and drain contacts. The reference contact (front-gate contact) with the electrolyte is implemented with a metal contact with a workfunction of 4.2 eV. The surface of the graphene layer is 500 nm × 500 nm, being the active area (area exposed) equals to 400 nm × 450 nm. Although in the actual device the graphene layer is deposited on top a SiO_2/Si substrate, however, in the simulation, in order to save computational resources, the silicon substrate was not considered, but its effect was taken into account by tuning the work function of the back-gate electrode, which, in our simulation is directly in contact with the 90 nm-thick SiO_2 layer. The work function of the back-gate electrode was assumed to be 4.6 eV.

Sentaurus TCAD is designed for the simulation of 3D semiconductors and graphene it is not included in the material library. We have adapted the parameter input file of a generic semiconductor material to properly model the bandstructure and transport parameters of an infinite ideal graphene monolayer. Thus, we have assumed a zero-bandgap semiconductor with a linear density of states relationship in both the conduction and valence bands near the edge of the bands (up to 0.5 eV). To do so, we used a multivalley approach with a non-parabolicity correction to mimic the graphene band structure (SentaurusTM Device User Guide, 2022).

To be operated as a biosensor, the GFET must work with a liquid gate, formed by an electrolyte and a metallic reference contact. The Synopsys Sentaurus platform lacks a model for an electrolyte. We had considered again a generic semiconductor material and particularize its physical parameter file with the characteristics of the electrolyte we used in our experimental setup, which is a diluted (0.001X) phosphate-buffered-saline solution (PBS). In accordance with Welch et al., (2013), the parameters chosen for simulating the diluted electrolyte were a bandgap of 1.5 eV and a relative permittivity set at 80 to align with the characteristics of water. The mobility of "electron" and "holes" was set to the values for Cl^- and Na^+ ions in water 6.88×10^{-4} and 4.98×10^{-4} $cm^2\ V^{-1}s^{-1}$, respectively (Chung et al., 2012). For the electron affinity we considered 3.9 eV and for the recombination lifetime of electrons ($1 \times 10^{-3}\ s^{-1}$) and holes ($1 \times 10^{-3}\ s^{-1}$) respectively. With these values the electrical characteristics of the fabricated pristine liquid-gate GFETs are reproduced as shown in the supplementary documentation.

In a GFET sensor as in any electron device, we can control the flow of carriers through it by means of electric or magnetic fields or by modulating the height of potential barriers. The signature of any electron device is its I–V characteristics, which represent the current flowing into its terminals as a function of the voltage applied to them. Therefore, to replicate the behaviour of a transistor, we need to calculate the current in the terminals for each of the combination of voltages applied to those terminals.

In the drift-diffusion approximation, the current density at any point in the device must be calculated for each type of carrier (electrons and holes). This calculation takes into account both the drift component, which is proportional to the local electric field and the concentration of carriers (electrons or holes at that point), and the diffusion component, which is proportional to the gradient of carrier density. Consequently, to evaluate the current, we need to determine the local electric field and the carrier concentrations at each point in the device. Therefore, the equations that the TCAD simulator must solve at each point of the device to calculate the electric field and carrier concentration are the continuity equations for each carrier and the Poisson equation to determine the electrostatic potential. These equations must be solved self-consistently.

2.3. Fabrication of graphene-based sensing devices

Graphene was synthesized through low-pressure chemical vapor deposition (LPCVD) where a polycrystalline copper foil was used as catalytic substrate. The reaction was made at 1 Torr using high-purity methane (CH_4) as a carbon precursor. The foils were first heated up to 1000 °C in a hydrogen (H_2) environment to reduce the native copper oxide on the copper foil surface. Then, a H_2/CH_4 gas mixture (50 sccm: 30 sccm) was added during the graphene growth at 1000 °C for 30 min. The cooling down step was made by opening the furnace, keeping constant the gas flow composition. Later, the graphene layers were transferred to cleaned quartz substrates using the PMMA based technique (Borin Barin et al., 2015). In this method, poly (methyl methacrylate) (PMMA) dissolved in anisole, was spin coated on top of the graphene films at 2000 rpm for 1 min. After coating, the samples were annealed at 80 °C for 10 min. Then, the samples were immersed in ferric chloride for 30 min to etch the copper foil. The resulting PMMA/-graphene films were floated on the surface of the aqueous solution. The suspended films were rinsed three times with deionized water followed by hydrochloric acid (10%) and deionized water again to remove any residual copper etchant. Finally, the graphene/PMMA stacks were transferred to cleaned quartz substrates. The PMMA film was removed with an acetone bath at 50 °C for 20 min. After that, the samples were rinsed with isopropanol and dried with nitrogen. In order to remove any PMMA residues and clean the graphene surface, the samples were annealed in a furnace at 300 °C in an Ar/H_2 atmosphere for 1 h.

After graphene deposition, reactive-ion etching (RIE) at 10 W and 30 sccm of O_2 was used to pattern the graphene employing a hardmask. Up to six sensors were fabricated on each substrate. Then, the Cr (5 nm)/Au (100 nm) electrodes were deposited by physical vapor deposition (thermal evaporation in high-vacuum environment). Finally, a laser treatment was performed onto the graphene layer using a computer-controlled laser engraver (XY plotter controlled by a ATmega2560-based micro control board) equipped with a blue diode laser (445 nm). The irradiation protocol (light power and speed) has been previously described by Ávila et al., (2022) demonstrating inter-device variability improvements. Briefly, the treatment consists of 4 cycles of

laser irradiation on the graphene surface. Once fabricated, the devices undergo electrical characterization using a saline solution to evaluate their performance. To achieve this, the transistor transfer curve (I_{DS}–V_G) is measured at a fixed value of $V_{DS} = 100$ mV after depositing a drop of buffered physiological-like solution (0.001X phosphate buffered saline (PBS)) to cover the graphene channel and using an Ag electrode as the gate contact (Fig. S2). The I_{DS}-V_G curve of the GFET exhibits a well-known V-shape, with a minimum current value reached at a specific gate voltage known as the Dirac point (V_{Dirac}) (Fig. S3). The position of the Dirac point depends on the pH and on the ionic concentration of the solution, so buffered solutions are preferred in order to keep the same pH from one measurement to another. This I_{DS}-V_G characterization allows extracting the value of the transconductance (g_m) of the transistor and gives access to the value of the V_{Dirac}. The transconductance of the transistor is a measure of how much the channel current changes in response to a change in the gate voltage, and it is evaluated as the derivative of the drain current versus the gate voltage. The transconductance is a crucial parameter that characterizes the amplification properties of the transistor. It indicates how effectively the transistor can convert changes in its gate-to-source voltage (V_G) into variations in the output current (I_{DS}). These parameters, g_m and V_{Dirac}, help to evaluate the quality of the technology process. Fig. S4 shows the I_{DS}-V_G and transconductance curves of 50 GFETs. The mean V_{Dirac} is 0.44 V with a standard deviation of 0.04 V. The mean value of the maximum of the normalized transconductance (g_m/V_{DS}) is 2.5 ms/V with a standard deviation of 0.3 ms/V. The mean field-effect mobility extracted from the transconductance (Mackin et al., 2014) has a value of 732 $cm^2V^{-1}s^{-1}$ for electrons and 900 $cm^2V^{-1}s^{-1}$ for holes. These values are in the range of the ones of other devices fabricated so far (Hébert et al., 2018).

2.4. GFET surface biofunctionalization

Graphene sensor areas were functionalized with an antibody specific for the detection of the SARS-CoV-2 Spike protein following two different approaches: a random *versus* site-selective antibody immobilization. In both cases, because of their ability to establish π-π interactions (non-covalent functionalization) with graphene and organic molecules, different pyrene-based derivatives were used as efficient probe linkers.

2.4.1. Random antibody immobilization

For random antibody immobilization, 1-Pyrenebutyric acid N-hydroxisuccinimide ester (PASE) was used. Briefly, each graphene sensor of the devices was incubated with 2 μL of different concentrations (10, 25, 50, 100, 200 and 500 μM) of PASE in dimethyl sulfoxide (DMSO) solution for different times (from 10 min up to 2 h). After that, they were rinsed twice with pure DMSO and twice with distilled water to remove unreacted molecules. Subsequently, the sensors were incubated different times (from 15 min up to 2 h) and under chamber humidity conditions with 5 μL of different solutions (2.5, 10 and 25 μg/mL) of Anti-SARS-CoV-2 spike antibody (Abcam) in 1X PBS. Then, they were rinsed twice with distilled water. To avoid the non-specific adsorption of other molecules on graphene, the unreacted sites were blocked with 5 μL of VTM for 15 min and rinsed twice with water. Finally, a polydimethylsiloxane (PDMS) microfluidic capsule was placed on the top of the device as explained in "Deposition of PDMS microfluidic capsule" section.

2.4.2. Site-selective immobilization

In the case of the site-selective immobilization, the 1-Pyrenebutyric hydrazide (PBH) was used to promote the orienting immobilization strategy. Sensors were incubated with 2 μL of a DMSO solution of PBH at different concentrations (200, 500, 1000, 1500 and 2000 μM) and times (from 10 min up to 2 h). After that, they were rinsed twice with DMSO and twice with distilled water to remove extra residues. To promote the oriented antibody attachment, we carried out the oxidation of its carbohydrate chains to generate aldehyde groups that finally permitted the specific imine-mediated coupling reaction with hydrazide residues of PBH previously adsorbed on graphene sensor area (Zhou et al., 2021). To promote the oxidation reaction of carbohydrate chains, sodium periodate ($NaIO_4$) was used. Briefly, 100 μL of a solution of Anti-SARS-CoV-2 spike antibody at 25 μg/mL concentration in 10 mM phosphate buffer (pH 7) were incubated with 10 μL of sodium periodate at 100 μM during 1 h under shaking and protected from light. Then, oxidized antibodies were recovered by ultrafiltration, washed trice with distilled water and resuspended in 10 mM phosphate buffer (pH 7.5) at different concentrations. Subsequently, sensors were incubated with 5 μL of oxidized antibody in 10 mM phosphate buffer (pH 7.5) solution, at different concentrations (2.5, 10 and 25 μg/mL), different times (from 15 min up to 2 h) and under chamber humidity conditions. After that, the functionalized sensors were rinsed twice with distilled water. To avoid the non-specific adsorption of other molecules, the antibody-modified graphene sensors were blocked with 5 μL of VTM for 15 min and then rinsed twice with water. Finally, the PDMS capsule was placed on top of the device as explained in "Deposition of PDMS microfluidic capsule" section.

2.5. Deposition of PDMS microfluidic capsule

After the surface biofunctionalization, the last step to complete the preparation of GFET biosensor was the placement of a PDMS capsule on top of the device. This capsule incorporates a fluidic design that distributes the liquid sample on the graphene active areas. The capsules consist of 0.7 mm wide channels through which the liquid samples are distributed on the different graphene biosensing surfaces. For the PDMS fabrication, the elastomer kit Sylgard 184 (Dow Corning) was used. The silicone-based elastomeric prepolymer and the curing agent were manually mixed for 5 min in a 10:1 ratio. In order to balance the hydrophobic nature of PDMS, Dimethylsiloxane Block Copolymer (Gelest) was added to the mixture (1% w/w) (Gökaltun et al., 2019; Miranda et al., 2021). After that, the blend was centrifugated at 2500 rpm for 5 min and degassed for 40 min. Next, the mixture was poured on a mould and cured at 80 °C for 2–3 h. After curing, the microfluidics devices were rinsed in isopropyl alcohol (IPA) and dried using a nitrogen jet. The capsules were glutted to the sensors using the one-part silicone adhesive 3140 RTV Coating (DOWSIL). The final devices were left overnight in ambient air to dry completely.

2.6. Characterization of functionalized sensors

In order to check the success of every step of biosensors functionalization and to characterize the final parameters, several physical, chemical, biochemical and electrical assays have been done.

2.6.1. Chemical and biochemical characterization of GFET surface functionalization

To quantify the amount of PASE and PBH adsorbed on the graphene surface, spectrophotometric quantification assays have been carried out. Briefly, spectral curves (λ = 245–400 nm analysis range) of the initially offered PASE or PBH solution and their relative supernatant (withdrawn incubation solution containing the not immobilized PASE or PBH amounts) have been compared. The peak area of each spectrum corresponds to the offered PASE/PBH moles or to the non-immobilized PASE/PBH moles, respectively. The percentage amount of PASE or PBH adsorbed on the graphene surface was obtained with the following equation: [peak area of supernatant/peak area initial solution] x 100. To assess the amount of oxidized and non-oxidated antibody attached to pyrenes, a Bradford or Micro BCA assays were carried out as described by the supplier (Thermofisher). Briefly, the concentration of antibody contained in the offered solution and in the supernatant (withdrawn incubation solution containing the not immobilized antibody amount) was calculated with each assay by using previously validated calibration

curves. Then, the percentage amount of antibody linked to pyrenes was obtained with the following equation: [antibody concentration in supernatant/antibody concentration of initial solution] x 100 and by comparing the offered blank with the supernatant after each incubation.

2.6.2. Raman spectroscopy

Raman spectrum of pristine and PASE/PBH-functionalized graphene was carried out in a Witec alpha300 equipment at 532 nm laser excitation. The laser power was set to 20 mW and an objective of 100× and 600 l per mm were used. All spectra were accumulated for 50 times.

2.6.3. X-ray photoelectron spectroscopy

The surface composition of the pristine graphene and the functionalized graphene with PASE, PASE + Antibody, PBH and PBH + antibody was analyzed by using X-ray photoelectron spectroscopy (XPS). Measurements were performed using a Kratos Axis Ultra-DLD spectrometer with Al Kα (1486.6 eV) radiation.

2.6.4. AFM

Atomic Force Microscopy (AFM) was employed to measure the surface topography of graphene before and after each functionalization step (pristine graphene, after antibody incubation, and after virus incubation) in order to compare the differences between random and oriented antibody immobilization. The measurements were performed using a NT-MDT Ntegra microscope in tapping or semi-contact mode (AM-AFM). The scanning was performed using an NSG01 (Spectrum Instruments) probe for noncontact/semicontact modes (tip curvature radius smaller than 10 nm, resonant frequency 87–230 kHz, force constant 1.45–15.1 N/m). The scanning area was 10 μm × 10 μm with a resolution of 256 x 256 points and a scanning frequency of 1 Hz.

2.6.5. Electrical measurements

To confirm the surface functionalization and in which extent the different immobilization strategies have impacted on the final electrical conductivity, the characteristic curves (I_{DS}-V_{GS}; DS: drain-source, GS: gate-source) and the Dirac point (V_{Dirac}) for each different functionalization steps were studied. These measurements were acquired using a Keysight B1500A semiconductor analyzer. The source-drain voltage (V_{DS}) was fixed at 50 mV and the electrolyte gate was swept from 1 to 0 V at a sweeping rate of 8 mV/s. The metal gate electrode was performed employing a silver wire and the liquid gate was generated with a diluted (0.001X) PBS solution.

2.6.6. Scanning Electron Microscopy

Scanning Electron Microscopy (SEM) was performed to observe graphene surface after virus incubation carried out with oriented and randomly biofunctionalized GFET sensors. Secondary electrons imaging was performed in a Tescan Vega 3 scanning electron microscope at 15 keV.

2.7. SARS-CoV-2 biosensing measurements

Electrical measurements were acquired using a Keysight B1500A semiconductor analyzer. The source-drain voltage (V_{DS}) was fixed at 50 mV and the electrolyte gate was swept from 1 to 0 V at a sweeping rate of 8 mV/s. The metal gate electrode was performed employing a silver wire. The sensors were measured before and after the incubation with each virus sample, consisting of each device in six sensors. The liquid gate solution was generated with a diluted (0.001X) PBS solution. Briefly, three measurements of each sensor were taken after PDMS capsule placement. Different dilutions at known concentrations from a commercially available SARS-CoV-2 stock solution of heat inactivated virus (from ATCC) were prepared in VTM. Each biofunctionalized sensor was incubated for 1 h with 100 μL of each virus dilution offered through the microfluidic channel of the PDMS capsule. After the incubation, the sample was removed, the sensors were rinsed twice with distilled water and, the final three electrical measurements for each sensor were performed. The Detection Limit (DL or LoD) and Quantitation Limit (QL or LoQ) values were calculated following the 'Validation Of Analytical Procedures Q2 (R2)' guidelines published by the 'International Council for Harmonisation of Technical Requirements for Registration of Pharmaceuticals for Human Use (ICH)' and adopted by both European Medicines Agency (EMA) and U.S. Food and Drug Administration (FDA) (ICH Q2(R2) Validation of analytical procedures - Scientific guideline, 2022a; Q2(R2) Validation of Analytical Procedures, 2022b). In this case, the validation of the lower range limits has been estimated using the approach based on the standard deviation of a linear response and a slope.

3. Results and discussion

3.1. In-silico simulation

As previously highlighted, the key scope of this work is to demonstrate the paramount relevance of the precise control of the GFET surface biofunctionalization as critical parameter (especially in terms of antibody orientation and distribution) to exalt the intrinsic properties of graphene while leading to a highly improved biosensing detection.

To begin the assessment of our hypothesis and to anticipate potential scenarios for each immobilization strategy, prior to experimental surface modification of the GFET sensors, an *in-silico* simulation study was carried out. For this purpose, a schematic simulated sensor was generated (Fig. S2). The simulated device consists of a graphene monolayer on top of a 90 nm-thick SiO_2 substrate. To be operated as a biosensor, the GFET has to work with a liquid gate, formed by an electrolyte and a metallic reference contact. In this case, the electrolyte is a diluted PBS solution (0.001X). After that, the output (I_D-V_D; I_D: drain current, V_D: drain voltage) and transfer (I_D-V_{FG}; I_D: drain current, V_{FG}: front-gate voltage) characteristics of the simulated liquid-gate GFET transistor, which reproduces the observed experimental behaviour of these devices, were calculated (Fig. S3) (Ávila et al., 2022).

The I_D-V_{FG} curve of the GFET exhibits a well-known V-shape, with a minimum current value reached at a specific gate voltage known as the Dirac point (V_{Dirac}) (Schwierz, 2010). V_{FG} denotes the voltage applied to the front gate electrode, which is the terminal in contact with the electrolyte, as illustrated in Fig. S2. An additional gate electrode, referred to as the back gate electrode (depicted in Fig. S2), is also present and is in contact with the substrate. Both gate electrodes operate in a similar manner, as they are capacitively connected to the graphene layer (the channel), enabling them to modify the carrier concentration within the channel and thus influence the device's conductivity (Novoselov et al., 2004; Schwierz, 2010). It's important to note that unless otherwise stated, the back gate is maintained at ground potential.

Note that V_{Dirac} in these curves for pristine graphene is slightly drifted to the right and does not show at $V_{FG} = 0$ V. The reason for this behaviour is that the position of the point of minimum current or Dirac point depends on the workfunction of the front gate electrode. In an ideal GFET scenario where the workfunction of both graphene and the electrode is identical, the Dirac point will indeed align precisely at zero Volts.

In addition to the intrinsic properties of the synthesized graphene, the presence of charged elements on the graphene surface is another critical factor that impacts on the I–V characteristics of the GFET and, consequently, on the Dirac point. Under certain conditions, the shift of the Dirac point is proportional to the number of charges present on the graphene surface and, consequently, to the concentration of the target analyte in the sample (Kwong Hong Tsang et al., 2019).

Thus, after tuning our simulation platform for the study of liquid gate GFETs, we proceeded to evaluate the impact on the I_D-V_{FG} characteristics of the GFET as a consequence of the biofunctionalization of graphene surface with bioreceptors, specifically the IgG anti-Spike protein SARS-CoV-2 antibody. The IgGs are large Y-shaped glycoproteins

(Fig. S5A) that can be assimilated to charged particles, and their charge (both module and sign) depends on the pH and composition of the electrolyte (Klein and Bjorkman, 2010; Wujcik et al., 2014).

To simulate the effect of the antibodies on the I–V characteristics of the GFET, we represented them as charged cubic boxes (Fig. S5B) (Ohno et al., 2009). Representing the antibody within a simplified model is a necessary approach aimed at conserving computational resources in the TCAD simulator. More precise models of the IgG antibody would greatly limit the number of antibodies and antibody-protein complexes that can be considered in the simulations, as computational resources—both memory and computational time—exponentially increase since the accurate description of the antibody's shape requires a higher number of mesh points in calculations. In our simulations, we have considered up to 1000 antibodies and 1000 antibody-protein complexes. With a more complex description of the antibody molecule such simulations would not be possible. Thus, it is crucial to strike a balance between precision and the available computational resources for practical reasons. This entails maintaining a reasonable level of accuracy without compromising the production of reliable results that elucidate observed experimental behaviors. As outlined in our manuscript, our current TCAD simulations do not aim for an exact quantitative reproduction of experimental results but strive to provide qualitative explanations for observed behaviors.

The cubic boxes were randomly positioned at a height ranging between 0.5 nm and 1 nm above the graphene surface, which corresponds to the average length of pyrene-based linker molecules typically used to anchor the bio-receptor to the graphene surface. Considering the average height of an IgG (Fig. S5A) (Marciello et al., 2014), we represented the antibody bioreceptor as a cube with a side length of 10 nm, containing a trapped charge concentration of -1x10^{19} e/cm^3 (Fig. S5B).

The overall charge exhibited by the antibody is determined by its isoelectric point (pI), which primarily depends on the presence of ionizable amino acids within the antibody. If the pH of the surrounding environment is below the antibody's pI, then it will carry a net positive charge. Conversely, if the pH is above the pI, the antibody will carry a net negative charge (Hong Liu et al., 2021). For the simulation, we assumed a pI value of the antibody of 7 (Yang et al., 2019). Therefore, since the pH value of the simulation has been set up at 7.4 (pH value of PBS), the IgG will be negatively charged. IgG antibodies are relatively large biomolecules composed of hundreds of amino-acids, and their net charge is determined by the overall balance of positive and negative charges on the amino-acid residues. The net charge can vary and is influenced by factors such as the specific amino acid composition, pI value, and any modifications or conjugations present on the antibody (Yang et al., 2019). Experimental measurements or computational methods specific to the antibody in question would be needed to provide an accurate estimation of its net charge. This detailed characterization of the net charge is beyond the scope of the current simulation study, which aims to provide a qualitative discussion regarding the importance of antibody arrangement on the graphene surface. Considering that, we have assumed a net charge of ten negative elementary charges, i.e., −10 electrons, for each IgG antibody. To represent this charge within the cubic boxes of our model, given that the box has a side length of 10 nm, we have considered a three-dimensional charge concentration of -1x10^{19} e/cm^3.

Note that the net charge assumption mentioned (ten negative elementary charges) is a hypothetical value chosen for the purposes of the simulation study, and it may not reflect the accurate actual net charge of a specific IgG antibody against the Spike protein of SARS-CoV-2.

Representing the antibody within a cubic box is a necessary simplification aimed at conserving computational resources in our TCAD simulator. More precise models of the IgG antibody would limit the number of antibodies and antibody-protein complexes that can be considered, as computational resources—both memory and computational time—exponentially increase when accurately describing the antibody's shape requires a higher number of mesh points in calculations.

In any scenario, at an initial stage, the primary impact of the antibody on the conductivity of the GFET channel will mainly derive from its net charge rather than the specific distribution of charge along the antibody structure. To validate this assertion, we conducted multiple simulations to compare the effects resulting from different charge distributions within the antibody. One of the extreme scenarios involves an antibody operating as a vertical dipole with zero net charge, having a negative charge in the bottom F_C fragment and a positive charge in the upper F_{ab} branches (Fig. S5). Fig. S6 displays the I_{DS}-V_G curves of a GFET biosensor: one with no antibodies (solid line), another with 100 antibodies modeled as a vertical dipole with $\pm 1 \times 10^{19}$ e/cm^3 in down position (negative charge in upper half part of the antibody and positive charge in the lower half part, represented by the dotted line) and in up position (positive charge up and negative charge down, represented by the dot-dash line). The three curves almost coincide, confirming that the primary influence of the antibody charge on the electrical characteristics of the GFET biosensor is mainly determined by their net charge.

The charged cubes anchored at the GFET surface are expected to cause a shift in the I_D-V_{FG} characteristics of the biofunctionalized device, enabling different drifts of the V_{Dirac} with respect to the V_{Dirac} of the pristine device (without trapped charges). The direction of the I_D-V_{FG} curve drift will be determined by the sign of the charges bonded over the graphene surface. If the trapped charges are positive, the I_D-V_{FG} curve will drift to the left, whereas negative charges cause the drift to occur to the right (Fig. S7) (Béraud et al., 2021). Consequently, the overall drift will be directly influenced by the sign and net charge of each biomolecule, the number of biomolecules, and their relative spatial distribution.

Once the parameters related to the simulation of the biofunctionalization of the GFET sensor were established, we proceed to simulate the evolution of the I_D-V_{FG} curves as the number of antibodies anchored to the graphene surface increased. The simulation involved incrementally anchoring Abs biomolecules on the GFET surface, starting from the initial pristine graphene surface and gradually increasing up to 300 Abs, with each antibody contributing a negative charge of 10 electrons ($N_{charge} = -1x10^{19}$ e/cm^{-3}). As expected, the Dirac point values exhibited a proportional rightward shift in relation to the increasing amount of immobilized Abs (Fig. S8).

With these essential data at our disposal, we proceeded to evaluate the impact of the graphene surface biofunctionalization with 300 antibodies (1.2×10^{11} Abs/cm^2) by comparing the evolution of related electrostatic potentials among different scenarios. These scenarios included the pristine device without additional charges (Fig. S9), the GFET modified with 300 homogeneously distributed antibodies (Fig. S10), and the GFET modified with 300 randomly clustered antibodies (Fig. S11). In both cases of antibody biofunctionalization, the presence of locally charged antibodies led to a decrease in the electrostatic potential of the graphene surface and a change in the concentration of carriers (electrons and holes) within the graphene layer (Fig. S9 vs Fig. S10 and Fig. S9 vs Fig. S11). However, in the case of randomly clustered antibody distribution (Fig. S11), the negative impact on the electrostatic potential was significantly greater than in the case of homogeneously distributed antibodies (Fig. S10).

Besides considering the impact of the amount and distribution of charges resulting from the antibodies placed on the GFET surface, the control of their orientation and distribution during the immobilization process is another critical parameter to be considered (Makaraviciute and Ramanaviciene, 2013). As mentioned earlier, an antibody has a Y-shaped structure consisting of four polypeptides: two heavy chains and two light chains (Wujcik et al., 2014). The recognition event between the antibody and the analyte occurs at the top part of the two shorts arms of the Y-shaped molecule (Fab fragment, Fig. S5A). To be effective, all the antibodies should be linked to the surface through the long arm (Fc fragment, Fig. S5A), thereby exposing the two bioactive short arms for capturing the antigen.

However, depending on the immobilization strategy, the antibodies can be anchored to the graphene surface in different positions, resulting in different spatial orientations (Fig. S1) that will impact on the bio-recognition ability and, finally, on the biosensing activity of the GFET sensor (Fig. S1). Generally, there are two main approaches for antibody-based sensor surface preparation: random (or non-oriented) and site-selective (or oriented) antibody immobilization. The latter expects that the antibody molecule is directly anchored to the graphene surface through the heavy chain (Fc fragment), preventing flexibility and movement and leaving the two sensitive bioactive Fab fragments freely exposed toward the reaction medium for recognizing and capturing the specific antigen (the Spike proteins of SARS-CoV-2, in our case) (Fig. S1). On the contrary, in the non-oriented case, antibodies are linked to the graphene surface through different point of their surface and in different orientations, resulting in poor exposure of the bioactive Fab fragments for antigen capture (Fig. S1). Considering the specific case of GFET biosensing mechanism, the consequences of this situation will be a lower-recovered biological activity efficiency (as only a fraction of the antibodies will be immobilized in a bioactive form able to recognize the target antigen) and a reduced sensitivity (as the remaining non-oriented immobilized antibodies will shield and hinder the GFET surface, hampering its interaction with the charges of captured antigens). Additionally, as a result of the non-oriented immobilization of each Ab molecule over the graphene surface, antibodies are expected to form heterogeneous clusters, being concentrated only in certain areas (Gao et al., 2022). In contrast, when oriented functionalization is promoted, all the immobilized antibodies are expected to be linked by the same point of their surface and uniformly distributed across the entire sensor surface in an oriented and standardized manner, thereby enhancing the overall ability to recognize a specific target antigen (Vijayendran and Leckband, 2001). This scenario is of paramount importance for the performance of a GFET biosensor, particularly in terms of sensitivity and reproducibility.

Therefore, to mimic the behaviour of the oriented-functionalization case, we have simulated five different immobilization of 600 antibodies each one and in a random but homogeneously distributed way (Fig. 2A and Fig. S12).

After that, the I_D-V_{FG} characteristics for the five cases considered were calculated. All five curves exhibited a perfect overlap, regardless of the distribution of Abs on the GFET surface (Fig. 2A and Fig. S12).

On the other hand, to simulate the case of non-oriented immobilization, the 600 Abs were clustered in groups of 10, 20, 30 and 60 Abs and randomly distributed on the graphene surface (Fig. 2B and Fig. S13). For each cluster size, multiple configurations were simulated, and the corresponding I_D-V_{FG} curves were calculated for each non-oriented distribution (Fig. 2B and Fig. S13). To facilitate comparison, the I_D-V_{FG} curve corresponding to the oriented case was also included. The results clearly show that, despite the constant number of antibodies (600), there is a significant variation in the curves depending on the cluster size, number and position (Fig. 2B and Fig. S13). Additionally, even for clusters of the same size, the position of the relative Dirac points varied across the curves. This behaviour indicates poor *inter*-sensor reproducibility of the measurement, which is strongly dependent not only on the number and size of the clusters but also on their relative positions in each configuration.

Overall, the simulation results confirm as critical the control of the homogeneity of the antibodies surface distribution during the bio-functionalization step of a GFET sensor to enhance its biosensing performance and reproducibility. In this sense, to achieve the most homogeneous sensing surface possible, various parameters could be taken into account during the biofunctionalization step. However, for optimal results, the orienting immobilization strategy for antibodies in general and the carbohydrate-mediated immobilization strategy in particular have been demonstrated to be the most useful ones (Vijayendran and Leckband, 2001).

3.2. GFET fabrication and surface biofunctionalization studies

Based on the results obtained in the simulation study, we have decided to proceed with the experimental development of both random and oriented immobilization strategies on the GFET surface by following the general scheme for sensor synthesis and functionalization described on continuation (Fig. 3).

First, the graphene monolayer was synthesized on a copper foil using a low-pressure chemical vapor deposition (LPCVD) method. Subsequently, the graphene layers were transferred onto cleaned quartz substrates using a wet transfer technique. After the graphene transfer, oxygen plasma etching was employed to pattern the graphene using a hardmask. Au/Cr electrodes were then deposited onto the patterned graphene through physical vapor deposition, resulting in the fabrication of up to six sensors on each quartz substrate (Fig. 3). As a final step and with the aim of improving inter-device variability, a laser treatment was performed on the graphene (Fig. 3) (Ávila et al., 2022).

After the GFET sensor fabrication, we developed experimentally the different surface biofunctionalization strategies based on the simulation results. To enable the random immobilization of antibodies, we selected the widely applied strategy based on the use of 1-Pyrenebutyric acid N-hydroxysuccinimide ester (PASE) (Fig. 4A). In fact, the activated esters of this acid linker are able to react in a very non-specific way with any nucleophilic residue (*e.g.*, $-NH_2$ group of Lysine or –OH of Serine, Threonine or Tyrosine residues; Fig. S14A) exposed over the whole antibody surface (both Fab and Fc), thus, resulting in their random

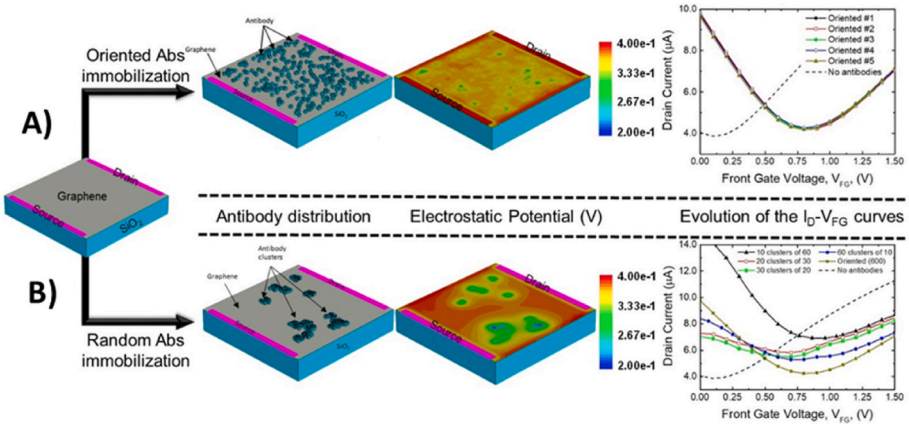

Fig. 2. Simulation of the impact of antibody distribution on graphene surface in both (A) oriented and (B) random immobilization. Five (n = 5) different simulations were carried out for each scenario.

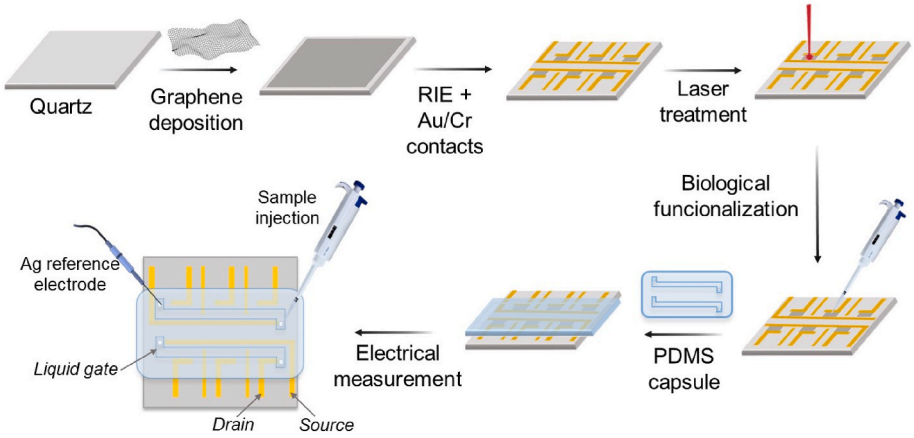

Fig. 3. Scheme of the fabrication, functionalization and characterization process of the described graphene-FET biosensors.

distribution on the graphene surface with all the possible spatial orientations described above (Fig. 4A and Fig. S1) (Zhou et al., 2021).

Conversely, to promote a simple, reproducible, and site-specific conjugation strategy able to enhance the standing directional immobilization of antibodies on the GFET while maximizing the surface homogeneity and consequently the biosensing ability, we decided to target the glycan chains located on the Fc surface of immunoglobulin G structure (Fig. S14B) (Vijayendran and Leckband, 2001). In fact, like many other mammalian proteins, IgGs are glycosylated on their surface and specifically at position 297 of the Fc region (Liu, 2015). This compositional difference between the Fab and the Fc fragments enables the design of site-selective immobilization strategies promoting the "tail-on" spatial orientations of Ab on the support surfaces while leaving the antigen-binding site (Fab fragments) completely exposed and unhindered (Fig. S1). As a result, the Abs correctly oriented on the GFET sensing surface will be able to effectively maintain their functional ability and to recognize specific antigens even at low concentrations. To enable the site-specific "tail-on" oriented immobilization of Abs through their glycan chains located in the Fc regions, firstly, we generated aldehyde reactive groups by oxidizing the carbohydrate molecules with sodium periodate (Fig. 4B). (Hoffman and O'Shannessy, 1988) The aldehyde groups can directly react with a hydrazide to form a covalent hydrazone bond through a nucleophilic addition. Therefore, we promoted this site-selective covalent bond formation by offering the oxidized IgGs to GFET surface previously modified with 1-Pyrenebutyric hydrazide (PBH) (Fig. 4B) (Marciello et al. 2013, 2014; Shen et al., 2017). It is noteworthy that the initial chemical modification of GFET surface has been carried out by using the same strategy (π-π stacking of pyrene-based linkers) in both cases (rBioGFET and oBioGFET). Consequently, any potential observed difference between both immobilization strategies could be related exclusively to the antibody orientation regardless to the used linker.

Different concentrations of both pyrene derivatives (from 10 up to 2000 μM) were incubated with the GFET sensors at different times (from 10 min up to 2 h (data not shown)) (Fig. S15).

In the case of PASE, the highest immobilization yield was achieved incubating the GFET surface with a 100 μM solution for 30 min. In these conditions, 4.7×10^{-11} mol of PASE per sensor were immobilized (Fig. S15A). The same experimental procedure was performed with PBH linker and the best result (1.1×10^{-9} mol of PBH immobilized per sensor) was achieved incubating the GFET surface with a 1000 μM PBH solution for 1 h (Fig. S15D). In both cases, testing higher concentrations of PASE or PBH, the amount of immobilized moles did not increase.

Afterward, various concentrations (from 2.5 to 25 μg/mL) of antibody (previously oxidized or not, depending on the intended immobilization strategy) were incubated with each pyrene modified GFET sensor (BioGFET). For the randomly oriented PASE-modified GFET sensor, a final immobilization of 3×10^{-13} mol of antibody per sensor was achieved using a 10 μg/mL solution after 1 h of incubation (rBioGFET) (Fig. 4A and Fig. S15B). In the case of oriented immobilization, 2.9×10^{-13} mol of oxidized anti SARS-CoV-2 spike antibody were immobilized on the PBH-modified GFET surface upon 1 h incubation with a 10 μg/mL solution (oBioGFET) (Fig. 4B and Fig. S15E). The incubation time for the oriented immobilization strategy was then studied in the range of 15 min to 2 h, and the best results were obtained after 30 min and 1 h of incubation for rBioGFET and oBioGFET, respectively (Fig. S15C and F). Under these conditions and for both immobilization strategies, a nearly identical amount of Anti-SARS-CoV-2 spike antibody was immobilized per sensor. This aspect is crucial when evaluating and comparing the influence of antibody orientation and distribution in virus detection.

3.3. Physical characterization of BioGFET sensors

In addition to the chemical and biochemical quantification of pyrene and antibody functionalization of the GFET surface, a comprehensive physical characterization was conducted to investigate the optimal conditions for each immobilization strategy. This characterization involved Raman spectroscopy, X-ray photoelectron spectroscopy (XPS), and Atomic Force Microscopy (AFM).

Initially, the biofunctionalizations mediated by both PASE and PBH were examined using Raman spectroscopy (Fig. S16). In pristine graphene, the Raman spectrum exhibits two prominent peaks, namely the G peak at 1580 cm^{-1} and the 2D peak at 2675 cm^{-1} (Fig. S16A). Following the surface chemical modification, the appearance of the D and D′ peaks PASE-modified graphene (Fig. S16B) and PBH-modified graphene (Fig. S16C) can be observed, indicating the successful chemical functionalization related to the presence of pyrene groups on the graphene surface.

Afterward, the characterization of each biofunctionalization step, starting with the pyrene modification and followed by the antibody immobilization, was carried out for both strategies (rBioGFET and oBioGFET) using XPS spectroscopy (Fig. S17). Fig. S17IA, IB and IC depict the C 1s spectra of pristine graphene, graphene modified with PASE and graphene modified with both PASE and antibody, respectively. On the other hand, Fig. S17IIA, IIB and IIC display the C 1s spectra of pristine graphene, graphene modified with PBH and graphene modified with both PBH and antibody, respectively. The binding energies were referenced to the C 1s peak at 285 eV. The fitting of the C 1s peak using a Gaussian-Lorentzian deconvolution reveals the presence of peaks corresponding to C–C peak (~285 eV), C–O–C (~286.5 eV), C–N (~286.8 eV) and C (=O)–O (~288.8 eV) depending on the specific case (Ederer et al., 2017).

The C 1s spectra of pristine graphene exhibit peaks corresponding to

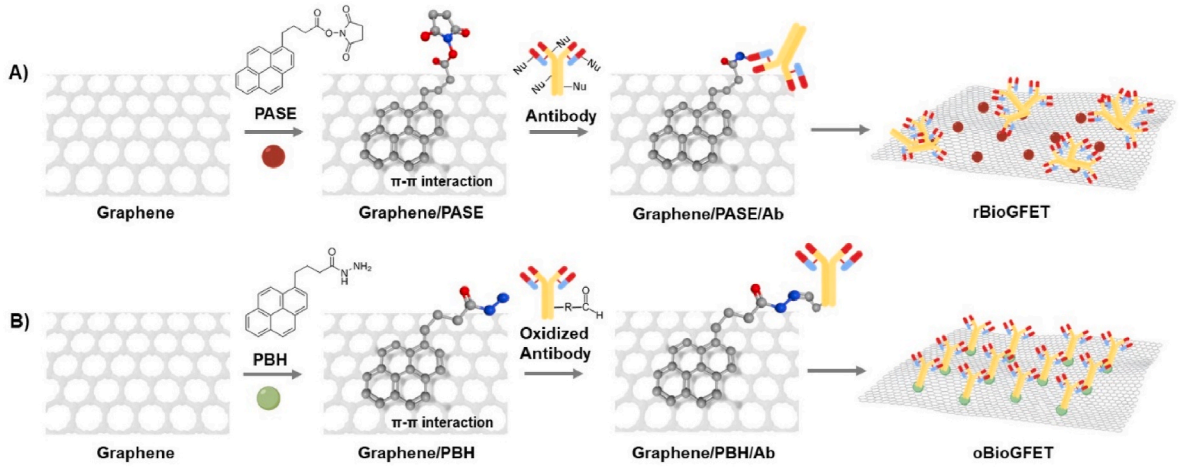

Fig. 4. General strategies applied to promote the A) random and B) oriented immobilization of antibodies over graphene surface.

C–C, C–O–C and C (=O)–O peaks. Upon functionalization of graphene with pyrene (PASE or PBH), a new peak corresponding to C–N appears, attributed to the nitrogen groups present in these molecules (Fig. S17IB and IIB). Additionally, a significant change in the spectrum is observed when graphene is functionalized with the antibody, leading to an increased contribution of the C–N and C (=O)–O peaks in the C 1s spectrum (Fig. S17IC and IICIC and S17IIC). This confirms the successful immobilization of antibodies on the graphene surface after functionalization.

Fig. S17ID and IID show the N 1s spectra of pristine graphene and functionalized graphene with PASE/PBH and PASE/PBH + antibody, respectively. The presence of pyrene and antibody is confirmed by the characteristic N 1s peak at~400 eV. In both cases, an increase in intensity of the N 1s peaks is observed upon the addition of the antibody to the pyrene. This effect can be attributed to the presence of a larger number of amide and amine groups on the antibodies compared to the one nitrogen atom per PASE and two nitrogen atoms per PBH molecule. It is worth noting that in Fig. S17ID, an additional peak emerges at~402 eV when PASE is added. This peak corresponds to the chemical structure of PASE with a (C-)O–N bond, whose binding energy is~402 eV. However, when the antibody is added, the peak shifts back to a C–N (-H) bond, resulting in a binding energy of~400 eV again.

Once the successful chemical modification and antibody bonding over the GFET surface were confirmed, a detailed surface analysis of pristine BioGFET sensors and both biofunctionalized sensors (rBioGFET and oBioGFET) was performed using AFM microscopy. This analysis aimed to evaluate the surface orientation and distribution of the immobilized antibodies in relation to each immobilization strategy. The results of this analysis are presented in Fig. S18.

After both immobilization strategies, the graphene surface appears to be covered with Anti-SARS-CoV-2 spike antibodies, but with different patterns depending on the applied technique. In the non-oriented functionalization, the antibodies are attached to the graphene surface in randomly distributed heterogeneous clusters, with heights ranging from 30 to 50 nm (Figs. S18B and D). In contrast, with the oriented strategy, the antibodies appear more uniformly distributed on the graphene surface and exhibiting a relatively consistent average height of 10 nm (Figs. S18C and D). Considering that the Anti-SARS-CoV-2 spike antibody is a Y shaped immunoglobulin with an approximately 10 nm height (Fig. S5, PDB file 1IGT) (Marciello et al., 2014), the obtained results confirm that our orienting immobilization strategy allows for the promotion of a standing orientation and uniform distribution of the target antibodies. Therefore, in comparison to the random and heterogeneous clustering strategy, this optimized biofunctionalization of GFET surface is expected to enhance the biorecognition activity of antibodies and, consequently, improve the sensitivity of virus detection.

3.4. Electrical characterization of BioGFET sensors

Toward this scope, in addition to the chemical, biochemical and physical characterizations, the impact of the different functionalization steps on the graphene conductivity was assessed by studying the characteristic I_{DS}-V_{GS} curves (Fig. S19).

During the non-oriented functionalization (Fig. S19B), the Dirac point (V_{Dirac}) shifted from 0.481 V to 0.275 V upon PASE functionalization. With the addition of the antibody, the V_{Dirac} further shifted to 0.280 V. On the other hand, during the oriented functionalization (Fig. S19C), V_{Dirac} shifted from 0.443 V to 0.313 V after modification with PBH. When the antibody was added, the V_{Dirac} switched to 0.361 V. Additionally, during the random antibody immobilization step, a vertical shift of the curves is observed, denoting an increase in the sensor current (Fig. S19B). Interestingly, this shift is not observed during the electrical measurements carried out on the oBioGFET. This behaviour indicates a higher sensor current in the randomly functionalized GFET sensors which is compatible with the non-uniform charge distribution on the GFET surface. Therefore, these experimental findings confirm the simulation predictions conducted at the beginning of this work (Fig. 2) as well as the direct characterization of BioGFET surface carried out by AFM microscopy (Fig. S18).

After the physicochemical characterization of the differently biofunctionalized GFET sensors, we proceeded with the characterization of their analytical response during the virus biosensing as a function of the different biofunctionalization techniques. Since the virus sample, as well as the real clinical samples obtained from naso- or oropharyngeal swabs, are prepared using Virus Transport Medium (VTM), we decided to incubate the biofunctionalized GFET sensors with this medium. To minimize any potential non-specific adsorption during the measurement of virus samples and to ensure optimal performance during the biosensing step, the biofunctionalized graphene surface was passivated and blocked. To achieve this, the biofunctionalized GFET sensors were incubated with pure VTM for 15 min, and the I_{DS}-V_{GS} curves and V_{Dirac} point were measured before and after this surface blocking process. As shown in Fig. S20, a variation of 0.099 V and 0.158 V in V_{Dirac} was observed for the random (Fig. S20A) and oriented (Fig. S20B) functionalization, respectively. This difference in the GFET response can be attributed to various factors. The composition of VTM, which predominantly consists of fetal bovine serum (FBS) containing proteins, especially bovine serum albumin (BSA), plays a significant role. BSA has an isoelectric point of 4.5–5 (Raghuwanshi et al., 2020), resulting in a negative charge at the VTM pH of 7.4, the pH at which incubation takes place. In the case of random functionalization of the GFET surface, after NHS hydrolysis of the unreacted PASE molecules, the surface will have pyrene butyric acid molecules with a pKa values of 4.76. As a result, the

surface becomes negatively charged at the VTM pH. On the other hand, in the case of oBioGFET, the presence of aminated PBH with a pKa value of 13 results in a positively charged surface at the VTM pH value of 7.4. This positive charge facilitates a higher adsorption of the negatively charged biomolecules, primarily BSA, present in the VTM medium. Consequently, this leads to a greater shift in ΔV_{Dirac}.

Finally, before proceeding with virus detection, we decided to analyze the time-dependent electrical stability of both random and oriented sensors in the presence of the liquid gate of our graphene field-effect transistor. For this purpose, the biofunctionalized and blocked devices (rBioGFET and oBioGFET) were incubated with 0.001X PBS solution to investigate potential changes in the I_{DS}-V_{GS} curves and Dirac point over time. As shown in Fig. S21, no significant shifts in V_{Dirac} values were observed in both cases after 1 h of incubation with the 0.001X PBS solution. More specifically, a mean shift of 0.021 V (8.4%) and 0.0245 V (7.5%) in V_{Dirac} values were observed for random and oriented GFET sensors, respectively. Additionally, a more long-term electrical stability was evaluated by measuring the BioGFETs after 7 days incubation with diluted (0.001X) PBS solution. With respects to the values obtained after 1 h incubation, a mean shift of 0.018 V (CV: 6.6%) and 0.007 V (CV: 1.4%) in V_{Dirac} values were observed for random and oriented GFET sensors, respectively. This result indicates an overall good electrical stability of functionalized GFET sensors, which is a crucial characteristic for field-effect transistor-based biosensors.

3.5. Characterization of biosensing performances of BioGFET sensors in SARS-CoV-2 detection

After the successful chemical, physical and electrical characterization of GFET biosensors produced by random *vs* oriented immobilization of anti-Spike protein antibodies, the sensors underwent biological preclinical validation by detecting SARS-CoV-2 in simulated clinical samples. In clinical settings, COVID-19 diagnosis is performed using nasopharyngeal swabs suspended in VTM. To accurately simulate real-world scenarios, we evaluated the response of the BioGFET sensors to the virus in undiluted VTM samples. The VTM contains various reagents that may affect the performance of the FET sensor (Centers for Disease Control and Prevention, 2019). For this purpose, we used a titrated commercial solution of SARS-CoV-2 virus (strain: USA-WA1/2020, ATCC) derived from direct culture supernatant from Vero E6 cells and we added the virus from the stock solution to the VTM buffer in controlled increasing concentrations, thus creating a calibration curve. The use of direct viral culture supernatant is accepted by the World Health Organization (WHO) for the development of diagnostic tools as it is considered a standardized protocol for evaluating the Limit of Detection (LoD) in antigen rapid diagnostic tests (Ag-RDTs) (Department of Health and Social Care, 2020; WHO & R&D Blue Print, 2020).

By this strategy, we have been able to successfully evaluate the sensitivity of both BioGFET sensors by establishing a correlation between the obtained conductivity data and the corresponding SARS-CoV-2 virus concentrations (Fig. 5).

In both scenarios, the outcomes demonstrated that the BioGFET sensors were capable of detecting SARS-CoV-2 viral particles in VTM, thereby, confirming the effectiveness of our biosensor in directly detecting viruses in simulated clinical samples without the need for preparation or preprocessing (Fig. 5A-C). Interestingly, by measuring SARS-CoV-2 samples previously incubated in VTM, a negative shift in V_{Dirac} is observed for both sensors, therefore, indicating that the viral particles appear positively charged (Fig. S7). However, considering that the measured isoelectric point of SARS-CoV-2 (strain: USA-WA1/2020) is 5.2 (Areo et al., 2021) and that the pH of VTM is 7.4, a negative surface potential of SARS-CoV-2 viral particle with a consequent rightward positive shift in V_{Dirac} value should be expected (Fig. S7). This observed behaviour agrees with research works that demonstrated as at pH environments (VTM: 7.4) above the isoelectric point (SARS-CoV-2: 5.2), the outer surface of virions is deprotonated, therefore, negatively charged and able to interact strongly with divalent and/or monovalent cations if present (Alhazmi et al., 2015; Joonaki et al., 2020). Effectively, VTM contains very high concentration of monovalent (*e.g.,* sodium chloride) and divalent (*e.g.* magnesium sulphate and calcium chloride) cations, therefore, confirming the positive surface charge of SARS-CoV-2 viral particles and the consequent leftward negative shift of V_{Dirac} during their biosensing with the BioGFET sensors (Fig. 5B and C).

Even though both sensors showed this similar general behaviour, the calibration curves depicting the BioGFET response (ΔV_{Dirac}) to increasing virus concentration in VTM exhibited significant differences between non-oriented and oriented antibody immobilization strategies (Fig. 5D vs Fig. 5E). In fact, in the case of oBioGFET, the results demonstrated a significant and linear ΔV_{Dirac} shift with the addition of the different virus solutions (Fig. 5E). Based on the collected data, the detection of the SARS-CoV-2 virus in VTM using oriented-BioGFET sensors exhibited a Limit of Detection (LoD) value of 1.9×10^2 plaque forming units (pfu)/ml, a Limit of Quantification (LoQ) value of 5.78×10^2 pfu/ml (ICH Q2(R2) Validation of analytical procedures - Scientific guideline, 2022; Q2(R2) Validation of Analytical Procedures, 2022) and the normalized response curve was linear with a coefficient of determination (R^2) value of 0.9943 in the concentration range of 1.9×10^2 to 2.85×10^3 pfu/mL (Fig. 5E). Interestingly, the LoD value achieved by the oriented BioGFET sensor met the predefined performance criterion of an analytical LoD of $\leq 5.0 \times 10^2$ plaque forming units (pfu)/ml as set by the WHO and international standards for accepting and ensuring the reliability of antigen tests (Department of Health and Social Care, 2020, WHO & R&D Blue Print, 2020).

Furthermore, it is worth noting that the LoD value showed by our oBioGFET is closely similar to that reported by the most sensitive commercially available Antigen RDTs (*e.g.,* BinaxNow Ag, Espline, Mologic, Sure-Status, Excalibur or Roche), all of which exhibit LoD values comprised within the range of $0.5–5 \times 10^2$ pfu/ml calculated in direct culture matrix (according to the WHO criteria) (Cubas-Atienzar et al., 2021). The biosensing performances of our oBioGFET sensor were similar or even better than other similar studies reported in literature (Table S1).

On the other hand, the calibration curve obtained from the randomly functionalized BioGFET under the same conditions and within the same concentration range yielded poorer analytical values. Specifically, within the same concentration interval, the randomly oriented BioGFET sensors exhibited a LoD value of 4.19×10^2 pfu/ml, a LoQ value of 1.27×10^3 pfu/ml and the normalized response curve was linear from 1.9×10^2 up to 1.8×10^3 pfu/mL with a R^2 value of 0.9802 (Fig. 5D). Considering that the Detection Limit (DL or LoD) and Quantitation Limit (QL or LoQ) are widely recognized as standard reference values for characterizing and defining the analytical sensitivity of every clinical laboratory test (2022a; 2022b; Tholen et al., 2004), our results collectively demonstrate that the SARS-CoV-2 detection using oriented graphene-FET sensors (oBioGFET) is 2.2 times more sensitive compared to the same detection performed with randomly oriented graphene-FET sensors (rBioGFET).

To furtherly crosscheck the differences in biosensing response resulting from the random and orienting immobilization strategies of anti-SARS-CoV-2 spike antibodies on the GFET surface, we chose to characterize one sensor for each immobilization strategy using AFM and SEM after its use in detecting a known virus concentration (5800 pfu/ml) (Fig. 6).

In fact, due to the dimensions of the SARS-CoV-2 virus (a round-shaped structure with an approximate diameter of 0.1 μm) (Bar-On et al., 2020), both techniques are expected to enable the direct visualization of virus distribution on the GFET surface as a function of immobilization strategy. As depicted in Fig. 6, in AFM images, when virus recognition is promoted on rBioGFET sensors (Fig. 6Ai and Aii), heterogeneous virus clusters appear randomly distributed across the GFET surface. Additionally, the height of these clusters, ranging between 0.25 and 0.5 μm, demonstrates the uncontrolled formation of large

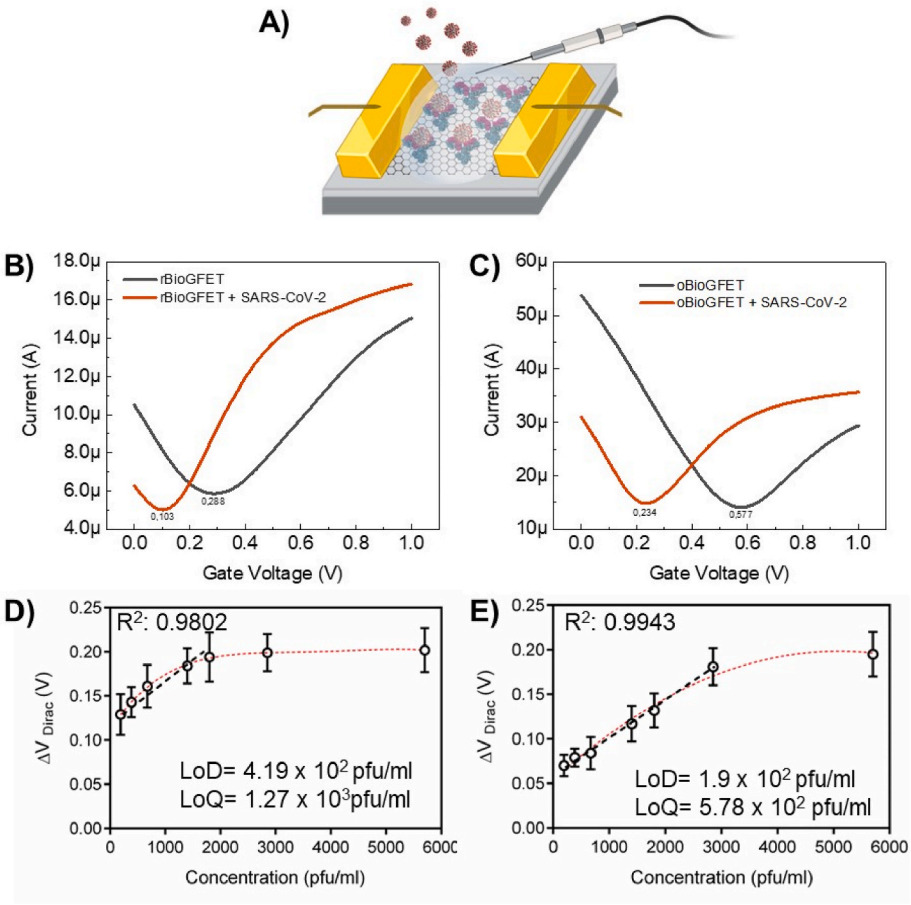

Fig. 5. (A) Schematic diagram of the aqueous-solution-gated GFET in antibody-conjugated graphene incubated with SARS-CoV-2. Representative I_{DS}-V_{GS} output curves of (B) random and (C) oriented functionalized sensors before and after incubation with SARS-CoV-2 (5800 pfu/ml) for 1 h. Dose-dependent response curve in the detection of SARS-CoV-2 virus in VTM solutions: (D) Random BioGFET; (E) Oriented BioGFET. Red dotted line: trend curve. Black long dashed line: linearity range. The error bars for (D) and (E) were calculated using data from four different chips (n = 4). The LoD and LoQ values were calculated using the 'standard deviation of a linear response and a slope' approach as described in 'Validation of Analytical Procedures Q2 (R2)' guidelines (published by the ICH and adopted by both EMA and FDA) (ICH Q2(R2) Validation of analytical procedures - Scientific guideline, 2022a; Q2(R2) Validation of Analytical Procedures, 2022) and as detailed in Materials and Methods.

antibody/virus aggregates (Fig. 6Aii). On the contrary, the AFM analysis of the oBioGFET sensors (Fig. 6Bi and Bii) revealed a much more uniform distribution and consistent height of each antibody/virus biocomplex. In this case, the mean height was generally within the range of 100–150 nm (Fig. 6Bii and Biv), which is consistent with the dimensions of a standing antibody (around 10 nm) *plus* a SARS-CoV-2 viral particle (around 100 nm). The SEM micrographs further confirmed these findings, clearly demonstrating a significant difference in surface homogeneity depending on the applied immobilization strategy (non-oriented: Fig. 6Aiii vs oriented: Fig. 6Biii).

Collectively, these results align with all the initial simulation predictions and indicate a substantial difference in conductivity and surface charge distribution based on the employed immobilization strategy and the resulting distribution of antibody/virus complexes on the sensors surface. As a result of this crucial difference, the I_{DS}-V_{GS} output curves of random (Fig. 5B) and oriented (Fig. 5C) BioGFET sensors during the SARS-CoV-2 detection exhibited distinct behaviours that agreed with the theoretical trends hypothesized during the simulation. Furthermore, the direct relationship between the antibody height (considered as the distance from bioactive Fab regions and graphene surface) and the increased biosensing sensitivity measured in low ionic (0.001X PBS) liquid-gated GFET is in agreement also with the Debye length (λ_D) theory (Kesler et al., 2020). The Debye length value (expressed in nm) can be defined as the distance from the sensing surface at which the potential of a net charge decays from its maximum value due to the screening effect of mobile ions in the medium. In other terms, if the electric charges related to the target analyte are located outside λ_D, they are considered out of range for electrostatic gating-based detection by a FET sensor and cannot be sensed properly. Among different parameters, λ_D is inversely related to medium ionic strength and, to increase it, the electrolyte ionic strength must be lowered. Under the sensing conditions here optimized (0.001X PBS and room temperature), the Debye length accounts for roughly 24 nm (Sultan et al., 2017). Therefore, in the case of oriented GFET biosensor, considering the antibody immobilization promoted in its standing orientation (around 10 nm height) and its homogeneous distribution (Figs. S18C and S18D), the λ_D will be large enough to permit to the graphene surface to sense the charges of captured SARS-CoV-2 viral particles, especially the charges related to the Spike protein (20 nm length) (Tai et al., 2021) outer layer (Fig. S22A).

Conversely, in the case of random GFET biosensor, considering the presence of differently oriented Abs and their heterogeneous clusters showing a height greater than the λ_D (Figs. S18B and S18D), many of the captured viral particle will be out of the Debye length, therefore, unable to contribute to the GFET sensing (Fig. S22B). As a result, the oBioGFET will be able to sense many more electrical charges from each captured viral particle than the rBioGFET, resulting in a more significant V_{Dirac} shift especially at low virus concentrations and, therefore, justifying its

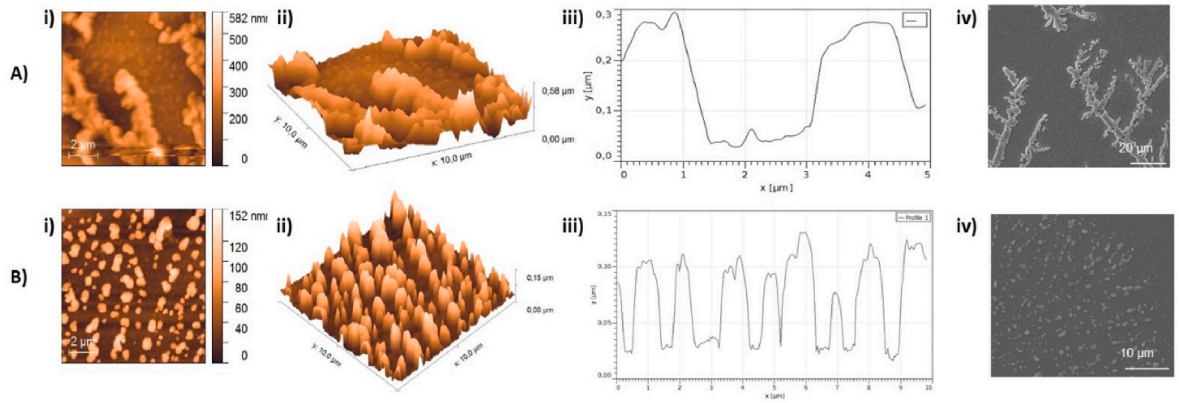

Fig. 6. Images of graphene surface after virus incubation on biosensors with (A) random functionalization and (B) oriented functionalization. AFM images (Ai-Aii), surface topography (Aiii) and SEM image (Aiv) of virus/randomly oriented antibody complex; AFM images (Bi-Bii), surface topography (Biii) and SEM image (Biv) of virus/oriented antibody complex.

biofunctionalization-related enhanced sensitivity (Fig. 5D vs Fig. 5E).

Consequently, all the chemical, physical and electrical characterizations provide clear confirmation of the paramount importance of controlling surface biofunctionalization (in terms of biomolecule orientation and homogeneity) to enhance the intrinsic physical properties of graphene-FET sensors and achieve a significantly more sensitive biosensing.

Finally, to confirm the absence of non-specific binding of virus particles, a SARS-CoV-2 non-specific human IgG antibody was used to functionalize the GFET surfaces under all optimized biofunctionalization conditions for both rBioGFET and oBioGFET. Biosensing was performed using a solution with the highest virus concentration (5800 pfu/ml). In both cases, no significant curve shift was observed, thereby confirming the absence of any non-specific virus particle adsorption in both BioGFET sensors (Fig. S23).

4. Conclusions

The hard lesson learnt from the COVID-19 pandemic has demonstrated that the availability of a widespread rapid, sensitive, reliable and easy-to-use diagnostic tool is a still unmet medical issue. The use of bidimensional nanomaterials such as graphene and their precise integration into *point-of-care* biomedical devices has emerged as a powerful alternative in diagnostic field. However, despite the progress of 2D nanomaterial-based biosensors, fundamental questions as how the control of surface biofunctionalization influences the sensing performance remain still unclear.

To address this challenge, in this work we have demonstrated that, in addition to its careful fabrication, the precise biofunctionalization of graphene sensor surface is another crucial factor for achieving enhanced biosensing performances.

Theoretical and experimental studies, (including *in-silico* simulation, AFM, SEM, XPS, Raman spectroscopy, biochemical techniques, bioorganic chemical reactions and electronic property characterization) were performed to forecast, design, characterize and elucidate the device's performance.

Taken together, the obtained results demonstrated that our GFET sensor can successfully detect SARS-CoV-2 virus in VTM samples. The sensor exhibits a very good LoD value which falls below the official threshold required by the WHO. It provides rapid detection without any sample pre-processing and offers a wide dynamic range. The oriented immobilization of antibodies and the consequent homogeneous modification of the sensor surface are critical for improving the sensor's response and increasing the sensitivity in virus detection by a 2.2 factor. In addition to its direct significance for COVID-19 pandemic surveillance, this work sheds light on an unexplored mechanistic aspect of bidimensional nanomaterial-based biosensor research. It offers general insights into the crucial role of biofunctionalization and its positive impact on the diagnostic capabilities of graphene biosensors and beyond. We envision that this strategy can potentially be extended to other types of biosensors based on 2D materials different from graphene, such as MoS_2 or WS_2 (Fathi-Hafshejani et al., 2021) opening up new possibilities for their application to other present (*e.g.,* early cancer detection) or future medical needs (*e.g.* forthcoming pandemics).

Associated content

The Supporting Information is available free of charge at:

Details on additional figures including different spatial orientations of antibodies, scheme of GFET sensor, I_D-V_{FG} curves for simulated GFET sensor, characterization of 50 pristine GFET sensors, immunoglobulin G scheme, simulated I_{DS}-V_G for a GFET biosensor with no antibodies anchored, I_D-V_{FG} curves depending on charges over GFET surface, I_D-V_{FG} curves depending on number of antibodies on the GFET sensor, electrostatic potential and electron density of pristine graphene, graphene decorated with homogeneously or random distributed antibodies, evolution of I_D-V_{FG} curves of distributed or clustered antibodies on graphene sensor, potential anchoring points of IgGs deppending on their orientation, optimization of functionalization parameters, Raman spectroscopy analysis, X-ray photoelectron spectroscopy analysis, AFM analysis of functionalized sensors, I_D-V_{FG} curves in different steps of functionalization, impact on V_{Dirac} after blocking with VTM, I_D-V_{FG} curves before and after incubation with PBS 0.001X, debye length with different immobilizations, I_D-V_{FG} curves of IgG funtionalized sensors before and after incubation with SARS-CoV-2 and analytical data of detection of SARS-CoV-2 reported in literature.

CRediT authorship contribution statement

Laura Lozano-Chamizo: Data curation, Formal analysis, Investigation, Methodology, Validation, Writing – original draft, Writing – review & editing. **Carlos Márquez:** Data curation, Investigation, Methodology, Visualization, Writing – original draft. **Marzia Marciello:** Data curation, Formal analysis, Investigation, Methodology, Writing – review & editing. **José Carlos Galdon:** Data curation, Formal analysis, Investigation, Methodology, Writing – review & editing. **Elsa de la Fuente-Zapico:** Data curation, Investigation, Methodology, Writing – review & editing. **Paula Martinez-Mazón:** Data curation, Investigation, Methodology, Writing – review & editing. **Víctor Gonzalez-Rumayor:** Data curation, Funding acquisition, Methodology, Writing – review & editing. **Marco Filice:** Conceptualization, Data curation, Formal analysis, Funding acquisition, Investigation, Methodology, Project administration,

Resources, Supervision, Writing – original draft, Writing – review & editing. **Francisco Gamiz:** Conceptualization, Data curation, Formal analysis, Funding acquisition, Investigation, Methodology, Resources, Software, Supervision, Writing – original draft, Writing – review & editing.

Declaration of competing interest

The authors declare that they have no known competing financial interests or personal relationships that could have appeared to influence the work reported in this paper.

Data availability

Data will be made available on request.

Acknowledgments

L.L.C., M.M., V.G.R. and M.F. would like to thank Comunidad de Madrid for the predoctoral grant IND2020/BIO-17523. M.F. is grateful to Instituto de Salud Carlos III (ISCIII) for project No DTS20/00109 (AES20-ISCIII) and PI22/00789 (AES22-ISCIII). L.L.C., M.F. and M.M. acknowledge the support of Microscopy & Dynamic Imaging Unit of CNIC, Madrid, Spain. The Unit is part of the ReDiB-ICTS and has the support of FEDER, "Una manera de hacer Europa." The CNIC is supported by the Instituto de Salud Carlos III (ISCIII), the Ministerio de Ciencia e Innovación (MCIN) and the Pro CNIC Foundation, and is a Severo Ochoa Center of Excellence (grant CEX 2020-001041-S funded by MICIN/AEI/10.13039/501100011033). The support of Spanish Ministerio de Ciencia e Innovación (MCIN) for funding the METALBIO Research Network (reference: RED 2022-134091-T) and the project CPP2022-009952 (MCIN/AEI /10.13039/501100011033, also funded by European Union NextGenerationEU/ PRTR) is acknowledged. M.M. and M.F. would like to thank Comunidad de Madrid for funding the REACT ANTICIPA-CM project. F.G. is grateful to Instituto de Salud Carlos III (ISCIII) for project No DTS20/00038, and Agencia Española de Investigación for research project PID 2021-128547OB-I00. The University of Granada group is also grateful to Junta de Andalucía for research projects P18-RT-4826, PYC-020-RE-023UGR, A-TIC-628-UGR20 (FEDER).

Appendix A. Supplementary data

Supplementary data to this article can be found online at https://doi.org/10.1016/j.bios.2024.116040.

References

Alhazmi, H.A., Nachbar, M., Albishri, H.M., Abd El-Hady, D., Redweik, S., El Deeb, S., Wätzig, H., 2015. A comprehensive platform to investigate protein-metal ion interactions by affinity capillary electrophoresis. J. Pharm. Biomed. Anal. 107, 311–317.

Alnaji, N., Wasfi, A., Awwad, F., 2023. The design of a point of care FET biosensor to detect and screen COVID-19. Sci. Rep. 13 (1), 4485.

Areo, O., Joshi, P.U., Obrenovich, M., Tayahi, M., Heldt, C.L., 2021. Single-particle characterization of SARS-CoV-2 isoelectric point and comparison to variants of interest. Microorganisms 9 (8).

Ávila, J., Galdon, J.C., Recio, M.-I., Salazar, N., Navarro, C., Marquez, C., Gamiz, F., 2022. Improved Inter-device Variability in Graphene Liquid Gate Sensors by Laser Treatment, vol. 192. Solid-State Electronics.

Bar-On, Y.M., Flamholz, A., Phillips, R., Milo, R., 2020. SARS-CoV-2 (COVID-19) by the numbers. Elife 9.

Benzigar, M.R., Bhattacharjee, R., Baharfar, M., Liu, G., 2021. Current methods for diagnosis of human coronaviruses: pros and cons. Anal. Bioanal. Chem. 413 (9), 2311–2330.

Béraud, A., Sauvage, M., Bazán, C.M., Tie, M., Bencherif, A., Bouilly, D., 2021. Graphene field-effect transistors as bioanalytical sensors: design, operation and performance. Analyst 146 (2), 403–428.

Biagetti, G., Crippa, P., Alessandrini, M., Marino, D.D., 2023. Portable high-accuracy wireless acquisition system for graphene-based sensors. IEEE Sensor. J. 23 (15), 17011–17024.

Borin Barin, G., Song, Y., de Fátima Gimenez, I., Souza Filho, A.G., Barreto, L.S., Kong, J., 2015. Optimized graphene transfer: influence of polymethylmethacrylate (PMMA) layer concentration and baking time on graphene final performance. Carbon 84, 82–90.

Chen, F., Qing, Q., Xia, J., Tao, N., 2010. Graphene field-effect transistors: electrochemical gating, interfacial capacitance, and biosensing applications. Chem. Asian J. 5 (10), 2144–2153.

Chung, I.Y., Jang, H., Lee, J., Moon, H., Seo, S.M., Kim, D.H., 2012. Simulation study on discrete charge effects of SiNW biosensors according to bound target position using a 3D TCAD simulator. Nanotechnology 23 (6), 065202.

Cubas-Atienzar, A.I., Kontogianni, K., Edwards, T., Wooding, D., Buist, K., Thompson, C. R., Williams, C.T., Patterson, E.I., Hughes, G.L., Baldwin, L., Escadafal, C., Sacks, J. A., Adams, E.R., 2021. Limit of detection in different matrices of 19 commercially available rapid antigen tests for the detection of SARS-CoV-2. Sci. Rep. 11 (1), 18313.

Ederer, J., Janoš, P., Ecorchard, P., Tolasz, J., Štengl, V., Beneš, H., Perchacz, M., Pop-Georgievski, O., 2017. Determination of amino groups on functionalized graphene oxide for polyurethane nanomaterials: XPS quantitation vs. functional speciation. RSC Adv. 7 (21), 12464–12473.

Fathi-Hafshejani, P., Azam, N., Wang, L., Kuroda, M.A., Hamilton, M.C., Hasim, S., Mahjouri-Samani, M., 2021. Two-dimensional-material-based field-effect transistor biosensor for detecting COVID-19 virus (SARS-CoV-2). ACS Nano 15 (7), 11461–11469.

Filice, M., Marchal, J.A., Gámiz, F., 2021. Biosensors Based on Two-Dimensional Materials.

Gao, S., Guisán, J.M., Rocha-Martin, J., 2022. Oriented immobilization of antibodies onto sensing platforms - a critical review. Anal. Chim. Acta 1189, 338907.

Gökaltun, A., Kang, Y.B.A., Yarmush, M.L., Usta, O.B., Asatekin, A., 2019. Simple surface modification of poly(dimethylsiloxane) via surface segregating smart polymers for biomicrofluidics. Sci. Rep. 9 (1), 7377.

Hébert, C., Masvidal-Codina, E., Suarez-Perez, A., Calia, A.B., Piret, G., Garcia-Cortadella, R., Illa, X., Del Corro Garcia, E., De la Cruz Sanchez, J.M., Casals, D.V., Prats-Alfonso, E., Bousquet, J., Godignon, P., Yvert, B., Villa, R., Sanchez-Vives, M. V., Guimerà-Brunet, A., Garrido, J.A., 2018. Flexible graphene solution-gated field-effect transistors: efficient transducers for micro-electrocorticography. Adv. Funct. Mater. 28 (12), 1703976.

Hoffman, W.L., O'Shannessy, D.J., 1988. Site-specific immobilization of antibodies by their oligosaccharide moieties to new hydrazide derivatized solid supports. J. Immunol. Methods 112 (1), 113–120.

Hong Liu, A.Y., Song, Jiajun, Wang, Naixiang, Lam, Puiyiu, Li, Yuenling, Ka-wai Law, Helen, Yan, Feng, 2021. Ultrafast, sensitive, and portable detection of COVID-19 IgG using flexible organic electrochemical transistors. Sci. Adv. 7 (38).

Jiang, Z., Feng, B., Xu, J., Qing, T., Zhang, P., Qing, Z., 2020. Graphene biosensors for bacterial and viral pathogens. Biosens. Bioelectron. 166, 112471.

Joonaki, E., Hassanpouryouzband, A., Heldt, C.L., Areo, O., 2020. Surface chemistry can unlock drivers of surface stability of SARS-CoV-2 in a variety of environmental conditions. Chem 6 (9), 2135–2146.

Kang, H., Wang, X., Guo, M., Dai, C., Chen, R., Yang, L., Wu, Y., Ying, T., Zhu, Z., Wei, D., Liu, Y., Wei, D., 2021. Ultrasensitive detection of SARS-CoV-2 antibody by graphene field-effect transistors. Nano Lett. 21 (19), 7897–7904.

Kesler, V., Murmann, B., Soh, H.T., 2020. Going beyond the debye length: overcoming charge screening limitations in next-generation bioelectronic sensors. ACS Nano 14 (12), 16194–16201.

Klein, J.S., Bjorkman, P.J., 2010. Few and far between: how HIV may be evading antibody avidity. PLoS Pathog. 6 (5), e1000908.

Kohmer, N., Toptan, T., Pallas, C., Karaca, O., Pfeiffer, A., Westhaus, S., Widera, M., Berger, A., Hoehl, S., Kammel, M., Ciesek, S., Rabenau, H.F., 2021. The comparative clinical performance of four SARS-CoV-2 rapid antigen tests and their correlation to infectivity in vitro. J. Clin. Med. 10 (2).

Kwong Hong Tsang, D., Lieberthal, T.J., Watts, C., Dunlop, I.E., Ramadan, S., del Rio Hernandez, A.E., Klein, N., 2019. Chemically functionalised graphene FET biosensor for the label-free sensing of exosomes. Sci. Rep. 9 (1), 13946.

Lemme, M., Echtermeyer, T., Baus, M., Kurz, H., 2007. A graphene field-effect device. Electron Device Letters, IEEE 28, 282–284.

Li, Y., Zhu, Y., Wang, C., He, M., Lin, Q., 2019. Selective detection of water pollutants using a differential aptamer-based graphene biosensor. Biosens. Bioelectron. 126, 59–67.

Liu, L., 2015. Antibody glycosylation and its impact on the pharmacokinetics and pharmacodynamics of monoclonal antibodies and fc-fusion proteins. J. Pharmaceut. Sci. 104 (6), 1866–1884.

Lou, D., Ji, L., Fan, L., Ji, Y., Gu, N., Zhang, Y., 2019. Antibody-oriented strategy and mechanism for the preparation of fluorescent nanoprobes for fast and sensitive immunodetection. Langmuir 35 (14), 4860–4867.

Lu, R., Zhao, X., Li, J., Niu, P., Yang, B., Wu, H., Wang, W., Song, H., Huang, B., Zhu, N., Bi, Y., Ma, X., Zhan, F., Wang, L., Hu, T., Zhou, H., Hu, Z., Zhou, W., Zhao, L., Chen, J., Meng, Y., Wang, J., Lin, Y., Yuan, J., Xie, Z., Ma, J., Liu, W.J., Wang, D., Xu, W., Holmes, E.C., Gao, G.F., Wu, G., Chen, W., Shi, W., Tan, W., 2020. Genomic characterisation and epidemiology of 2019 novel coronavirus: implications for virus origins and receptor binding. Lancet 395 (10224), 565–574.

Mackin, C., Hess, L.H., Hsu, A., Song, Y., Kong, J., Garrido, J.A., Palacios, T., 2014. A current–voltage model for graphene electrolyte-gated field-effect transistors. IEEE Trans. Electron. Dev. 61, 3971–3977.

Maia, R., Carvalho, V., Faria, B., Miranda, I., Catarino, S., Teixeira, S., Lima, R., Minas, G., Ribeiro, J., 2022. Diagnosis methods for COVID-19: a systematic review. Micromachines 13 (8).

Makaraviciute, A., Ramanaviciene, A., 2013. Site-directed antibody immobilization techniques for immunosensors. Biosens. Bioelectron. 50, 460–471.
Marciello, M., Bolivar, J.M., Filice, M., Mateo, C., Guisan, J.M., 2013. Preparation of lipase-coated, stabilized, hydrophobic magnetic particles for reversible conjugation of biomacromolecules. Biomacromolecules 14 (3), 602–607.
Marciello, M., Filice, M., Olea, D., Velez, M., Guisan, J.M., Mateo, C., 2014. Useful oriented immobilization of antibodies on chimeric magnetic particles: direct correlation of biomacromolecule orientation with biological activity by AFM studies. Langmuir 30 (49), 15022–15030.
Miranda, I., Souza, A., Sousa, P., Ribeiro, J., Castanheira, E.M.S., Lima, R., Minas, G., 2021. Properties and applications of PDMS for biomedical engineering: a review. J. Funct. Biomater. 13 (1).
Novoselov, K.S., Geim, A.K., Morozov, S.V., Jiang, D., Zhang, Y., Dubonos, S.V., Grigorieva, I.V., Firsov, A.A., 2004. Electric field effect in atomically thin carbon films. Science 306 (5696), 666–669.
Ohno, Y., Maehashi, K., Yamashiro, Y., Matsumoto, K., 2009. Electrolyte-gated graphene field-effect transistors for detecting pH and protein adsorption. Nano Lett. 9 (9), 3318–3322.
Raghuwanshi, V.S., Yu, B., Browne, C., Garnier, G., 2020. Reversible pH responsive bovine serum albumin hydrogel sponge nanolayer. Front. Bioeng. Biotechnol. 8, 573.
Rexha, J., Perta, N., Roscioni, A., Motta, S., La Teana, A., Maragliano, L., Romagnoli, A., Di Marino, D., 2023. Unlocking the potential of field effect transistor (FET) biosensors: a perspective on methodological advances in computational and molecular biology. Advanced Sensor Research 2 (11), 2300053.
Romagnoli, A., D'Agostino, M., Pavoni, E., Ardiccioni, C., Motta, S., Crippa, P., Biagetti, G., Notarstefano, V., Rexha, J., Perta, N., Barocci, S., Costabile, B.K., Colasurdo, G., Caucci, S., Mencarelli, D., Turchetti, C., Farina, M., Pierantoni, L., La Teana, A., Al Hadi, R., Cicconardi, F., Chinappi, M., Trucchi, E., Mancia, F., Menzo, S., Morozzo della Rocca, B., D'Annessa, I., Di Marino, D., 2023. SARS-CoV-2 multi-variant rapid detector based on graphene transistor functionalized with an engineered dimeric ACE2 receptor. Nano Today 48, 101729.
Ruiz, G., Tripathi, K., Okyem, S., Driskell, J.D., 2019. pH impacts the orientation of antibody adsorbed onto gold nanoparticles. Bioconjugate Chem. 30 (4), 1182–1191.
Schwierz, F., 2010. Graphene transistors. Nat. Nanotechnol. 5 (7), 487–496.
Seo, G., Lee, G., Kim, M.J., Baek, S.-H., Choi, M., Ku, K.B., Lee, C.-S., Jun, S., Park, D., Kim, H.G., Kim, S.-J., Lee, J.-O., Kim, B.T., Park, E.C., Kim, S.I., 2020. Rapid detection of COVID-19 causative virus (SARS-CoV-2) in human nasopharyngeal swab specimens using field-effect transistor-based biosensor. ACS Nano 14 (4), 5135–5142.
Shen, M., Rusling, J., Dixit, C.K., 2017. Site-selective orientated immobilization of antibodies and conjugates for immunodiagnostics development. Methods 116, 95–111.
Sultan, S.M., de Planque, M.R.R., Ashburn, P., Chong, H.M.H., 2017. Effect of phosphate buffered saline solutions on top-down fabricated ZnO nanowire field effect transistor. J. Nanomater., 5413705, 2017.
Tai, L., Zhu, G., Yang, M., Cao, L., Xing, X., Yin, G., Chan, C., Qin, C., Rao, Z., Wang, X., Sun, F., Zhu, Y., 2021. Nanometer-resolution in situ structure of the SARS-CoV-2 postfusion spike protein. Proc. Natl. Acad. Sci. U. S. A. 118 (48).
Tam, J.O., de Puig, H., Yen, C.W., Bosch, I., Gomez-Marquez, J., Clavet, C., Hamad-Schifferli, K., Gehrke, L., 2017. A comparison of nanoparticle-antibody conjugation strategies in sandwich immunoassays. J. Immunoassay Immunochem. 38 (4), 355–377.
Tholen, D., Linnet, K., Kondratovich, M.V., Armbruster, D.A., Garrett, P.E., Jones, R.L., Kroll, M.H., Lequin, R.M., Pankratz, T., Scassellati, G.A., Schimmel, H.G., Tsai, J., 2004. Protocols for Determination of Limits of Detection and Limits of Quantitation. Approved Guidelines.
Vijayendran, R.A., Leckband, D.E., 2001. A quantitative assessment of heterogeneity for surface-immobilized proteins. Anal. Chem. 73 (3), 471–480.
Welch, D., Shah, S., Ozev, S., Christen, J.B., 2013. Experimental and simulated cycling of ISFET electric fields for drift reset. IEEE Electron. Device Lett. 34 (3), 456–458.
Wujcik, E.K., Wei, H., Zhang, X., Guo, J., Yan, X., Sutrave, N., Wei, S., Guo, Z., 2014. Antibody nanosensors: a detailed review. RSC Adv. 4 (82), 43725–43745.
Xu, L., Ramadan, S., Rosa, B.G., Zhang, Y., Yin, T., Torres, E., Shaforost, O., Panagiotopoulos, A., Li, B., Kerherve, G., Kim, D.K., Mattevi, C., Jiao, L.R., Petrov, P. K., Klein, N., 2022. On-chip integrated graphene aptasensor with portable readout for fast and label-free COVID-19 detection in virus transport medium. Sens Diagn 1 (4), 719–730.
Yang, D., Kroe-Barrett, R., Singh, S., Laue, T., 2019. IgG charge: practical and biological implications. Antibodies 8 (1).
Zhou, S., Hu, J., Chen, X., Duan, H., Shao, Y., Lin, T., Li, X., Huang, X., Xiong, Y., 2021. Hydrazide-assisted directional antibody conjugation of gold nanoparticles to enhance immunochromatographic assay. Anal. Chim. Acta 1168, 338623.
Zhu, C., Du, D., Lin, Y., 2015. Graphene and graphene-like 2D materials for optical biosensing and bioimaging: a review. 2D Mater. 2 (3), 032004.

Web references

Centers for Disease Control and Prevention, 2023. COVID Data Tracker. US Department of Health and Human Services, CDC, Atlanta, GA. https://covid.cdc.gov/covid-data-tracker.
Centers for Disease Control and Prevention. Preparation of viral transport medium. https://www.cdc.gov/coronavirus/2019-ncov/downloads/Viral-Transport-Medium.pdf.
Department of Health and Social Care, 2020. Protocol for Evaluation of Rapid Diagnostic Assays for Specific SARS-CoV-2 Antigens (Lateral Flow Devices) GOV.UK. In: https://www.gov.uk/government/publications/assessment-and-procurement-of-coronavirus-covid-19-tests/protocol-for-evaluation-of-rapid-diagnostic-assays-for-specific-sars-cov-2-antigens-lateral-flow-devices.
G7 pandemic preparedness partnership, 2021. 100 Days Mission to Respond to Future Pandemic Threats. https://assets.publishing.service.gov.uk/government/uploads/system/uploads/attachment_data/file/992762/100_Days_Mission_to_respond_to_future_pandemic_threats_3_.pdf.
SentaurusTM Device User Guide U-2022.12.
WHO & R&D Blue Print, 2020. Target Product Profiles for Priority Diagnostics to Support Response to the COVID-19 Pandemic v.1.0. https://www.who.int/publications/m/item/covid-19-target-product-profiles-for-priority-diagnostics-to-support-response-to-the-covid-19-pandemic-v.0.1.
WHO, 2023. COVID-19 Weekly Epidemiological Update. https://www.who.int/publications/m/item/weekly-epidemiological-update-on-covid-19—1-september-2023.
ICH Q2(R2) Validation of analytical procedures - Scientific guideline, 2022a. In: https://www.ema.europa.eu/en/ich-q2r2-validation-analytical-procedures-scientific-guideline#current-effective-version—currently-under-revision,-see-below-section.
Q2(R2) Validation of Analytical Procedures, 2022b. In: https://www.fda.gov/regulatory-information/search-fda-guidance-documents/q2r2-validation-analytical-procedures.